

Plasmoid-Induced Turbulence in Collisionless Magnetic Reconnection

Keizo Fujimoto^{1,*} and Richard D. Sydora²

¹*Division of Theoretical Astronomy, National Astronomical Observatory, 2-21-1 Ohsawa, Mitaka, Tokyo 181-8588, Japan*

²*Department of Physics, University of Alberta, Edmonton, Alberta T6G 2E1, Canada*

(Received 17 August 2012; revised manuscript received 25 September 2012; published 28 December 2012)

The dissipation mechanism in collisionless magnetic reconnection in a quasisteady period is investigated for the antiparallel field configuration. A three-dimensional simulation in a fully kinetic system reveals that a current-aligned electromagnetic mode produces turbulent electron flow that facilitates the transport of the momentum responsible for the current density. It is found that the electromagnetic turbulence is drastically enhanced by plasmoid formations and has a significant impact on the dissipation at the magnetic x -line. The linear analyses confirm that the mode survives in the real ion-to-electron mass ratio, which assures the importance of the turbulence in collisionless reconnection.

DOI: [10.1103/PhysRevLett.109.265004](https://doi.org/10.1103/PhysRevLett.109.265004)

PACS numbers: 52.35.Vd, 52.65.Rr, 94.30.ep

Magnetic reconnection is a ubiquitous phenomenon in the Universe, explosively releasing the magnetic field energy into plasma kinetic energy. While it occurs in a spatially localized region, the process changes the global field line topology and causes large-scale plasma convection, playing a crucial role in dynamical phenomena such as the geomagnetospheric substorms and solar flares. It has been a long-standing issue how the explosive magnetic dissipation is generated in collisionless plasmas where the frictional effect due to the binary collision is negligibly small. In fact, in the resistive magnetohydrodynamic framework based on the Spitzer conductivity, the rate of reconnection is unrealistically small to explain the explosive energy release [1,2]. In order to enhance the reconnection rate, the fluid models, in which the dissipation processes are not explicitly incorporated, employ numerical resistivity and/or *ad hoc* anomalous resistivity [3–6]. However, it has been suggested that the rate of reconnection depends on the resistivity model [3,4] and, in the global fluid simulations, the global responses of the substorms and flares are sensitive to the parametrization of the resistivity [5,6]. These fluid simulation results indicate that the dissipation processes have an impact on the macroscopic dynamics of reconnection and the relevant phenomena, while they proceed in a microscopic region around the magnetic x -line.

For two-dimensional (2D) reconnection, it has been demonstrated [7–9] that the momentum transport due to the Speiser-type motion of the electrons gives rise to the electron viscosity around the x -line which leads to an effective resistivity. Although the electron viscosity gives sufficient dissipation for supporting the reconnection electric field under the thin current layer on the order of the electron inertia length, such a thin current sheet has not been observed, neither in the laboratory experiments [10] nor in the geomagnetosphere [11]. The observations have also shown [12,13] that the intense activities of electromagnetic (EM) waves are usually detected around the

x -line in the frequency ranging from ω_{ci} to ω_{LH} , where ω_{ci} and ω_{LH} are the ion cyclotron frequency and the lower-hybrid frequency, respectively. These observational facts imply the existence of the anomalous momentum transport due to the wave activities that are not incorporated in the 2D systems [14]. Although three-dimensional (3D) kinetic simulations have been examined to investigate the impact of the current-aligned turbulence on the reconnection process [15–17], it has been difficult, because of the limitation of computer resources, to clarify what kind of waves arise and to what extent they contribute to the dissipation in quasisteady period. The importance of the EM turbulence was recently demonstrated for a configuration with intense guide field [18]. However, it is not straightforward that the same mechanism works for the antiparallel field configuration. Furthermore, large-scale kinetic simulations in 2D systems [19,20] have revealed that the structure of the electron current layer changes dynamically, that is, the electron layer is elongated in the downstream direction and is subject to plasmoid formations. The coupling process between such a dynamical structure change and the current-aligned turbulence has not been explored yet for the antiparallel configuration.

The present study investigates the dissipation mechanism in 3D collisionless reconnection during a quasisteady period for the antiparallel configuration that gives the most fundamental nature of the reconnection process. We have performed the EM particle-in-cell simulations in a 3D system. The simulation model [21] employs the adaptive mesh refinement and the particle splitting-coalescence method in order to achieve efficient high-resolution simulations. The system boundaries are periodic in the x and y directions, and the conducting wall in the z direction. The simulations are carried out using a Harris-type current sheet with the magnetic field $B_x(z) = -B_0 \tanh(z/\delta)$ and the number density $n(z) = n_0 \operatorname{sech}^2(z/\delta) + n_b \tanh^2(z/\delta)$, where δ is the half width of the current sheet. We choose $\delta = 0.5\lambda_i$ and $n_b = 0.044n_0$ with λ_i the ion inertia length

based on n_0 . Although there appears a weak pressure imbalance due to the background density profile, the equilibrium is quickly established without any significant modification to the current sheet structure. The ion-to-electron mass ratio and velocity of light are $m_i/m_e = 100$ and $c/V_A = 27$, respectively, where $V_A = B_0/\sqrt{\mu_0 n_0 m_i}$ is the Alfvén velocity. The temperature ratios are $T_{0i}/T_{0e} = 5.0$, $T_{bi}/T_{be} = 1.0$, and $T_{be}/T_{0e} = 1.0$, where T_{0s} and T_{bs} are the temperatures of the species s for the sheet and background plasmas, respectively. The system size is $L_x \times L_y \times L_z = 81.9\lambda_i \times 10.2\lambda_i \times 81.9\lambda_i$ that is entirely covered by the base level cells (the coarsest cells) with $\Delta_{L_B} = 0.08\lambda_i$ and can be locally subdivided into finer cells up to the dynamic range level with $\Delta_{L_D} = 0.02\lambda_i$, so that the highest spatial resolution is $4098 \times 512 \times 4098 \sim 10^{10}$. The large system size in the x direction enables us to pursue the long time evolution of the reconnection process. The refinement criterion is provided by the local electron Debye length λ_{De} and electron flow velocity V_{ey} , so that cells satisfying $\Delta_L \geq 2.0\lambda_{De}$ or $V_{ey} \geq 2.0V_A$ are subdivided.

Magnetic reconnection is initiated with a small perturbation to the magnetic field, which produces the x -line in the current-aligned direction at the center of the xz plane. Figure 1(a) shows a snapshot of the 3D simulation during a quasisteady fast reconnection with the reconnection rate $E_R \approx 0.1$. It is observed that the thin current layer formed around the x -line is unstable to plasmoid formation in the x direction and to a kink-type EM mode in the y direction. The reconnection rate [Fig. 1(b)] is evaluated using the electric field E_y at the x -line averaged over y and the negative time derivative of the unreconnected magnetic flux per length, both of which are normalized by the upstream values. One can see that both the evaluations are in good agreement and the fast reconnection has started at $t\omega_{ci} \approx 14$. Figure 1(c) presents the evolution of the wave number spectrum in the y direction around the x -line. As has been reported in earlier 3D simulations [15–17], the first growing mode is the lower hybrid drift instability peaking at $t\omega_{ci} \approx 4$ with $k_y\lambda_i \approx 10$ ($M_y \equiv k_y L_y/2\pi = 17$) which penetrates into the center of the current sheet around this time. However, it disappears from the vicinity of the x -line in the later time, so that it hardly affects the reconnection process during the quasisteady period. It is found that the activity of the EM mode with $k_y\lambda_i \approx 1.2$ ($M_y = 2$) dominates in the thin current layer during the fast reconnection, in particular, after $t\omega_{ci} \approx 16$ when the first plasmoid has been generated as shown later.

The EM mode produces turbulent electron flow around the electron current layer, which transports the electron momentum responsible for the current density, generating the magnetic dissipation near the x -line. The anomalous momentum transport due to the turbulence is evaluated in the generalized Ohm's law averaged over the wave structures

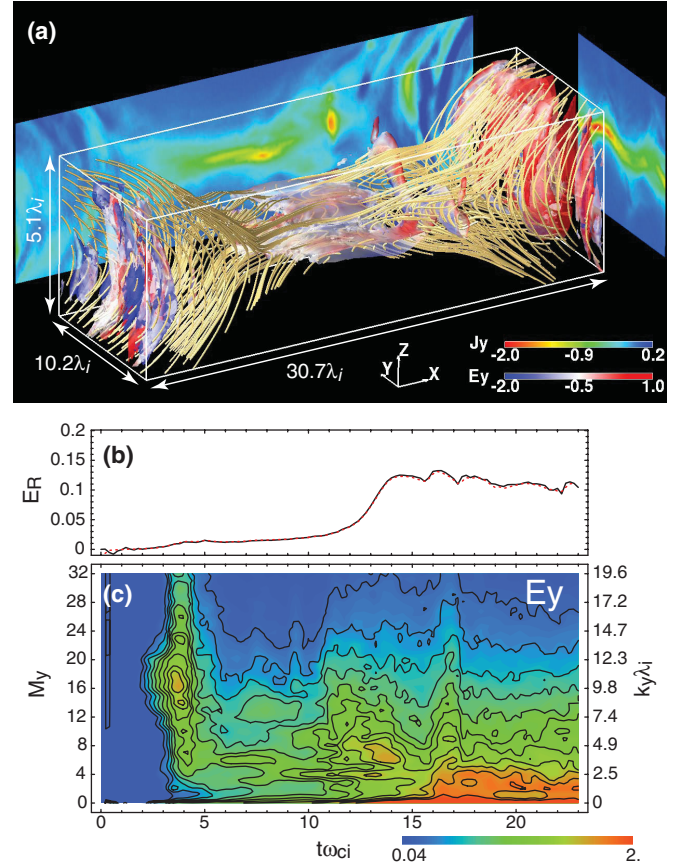


FIG. 1 (color). (a) 3D snapshot at $t\omega_{ci} = 23.0$ of an isosurface for $|J|/en_0V_A = 0.80$ colored by E_y with the magnetic field lines in yellow curves and 2D profiles of J_y at $x = 41.0\lambda_i$ (the center of the x system) and $y = 0.0$. (b) Time evolution of the reconnection rate E_R evaluated by $\langle -E_y \rangle$ at the x -line (black curve) and the negative time derivative of the unreconnected magnetic flux (red dotted curve). (c) Time evolution of the spectrum of the wave number k_y (equivalently the mode number $M_y \equiv k_y L_y/2\pi$) for E_y at the x -line.

$$\begin{aligned} \langle -E_y \rangle &= \frac{1}{\langle n_e \rangle} \langle (n_e \mathbf{V}_e) \times \langle \mathbf{B} \rangle \rangle_y + \frac{1}{e \langle n_e \rangle} \langle \nabla \cdot \mathbf{P}_e \rangle_y \\ &+ \frac{m_e}{e \langle n_e \rangle} \langle n_e \mathbf{V}_e \cdot \nabla V_{ey} \rangle + \frac{1}{\langle n_e \rangle} \langle \delta n_e \delta E_y \rangle \\ &+ \frac{1}{\langle n_e \rangle} \langle \delta (n_e \mathbf{V}_e) \times \delta \mathbf{B} \rangle_y, \end{aligned} \quad (1)$$

where $A \equiv \langle A \rangle + \delta A$ for a variable A with $\langle A \rangle = (1/L_y) \times \int_0^{L_y} A dy$ the average over the y axis so that $\langle \delta A \rangle = 0$, and \mathbf{P}_e is the electron pressure tensor. The anomalous effect due to the EM turbulence is represented by the last term of the right-hand side of Eq. (1). As shown in Fig. 2(a), the EM turbulence (red curve) has a significant impact on the magnetic dissipation at the x -line (i.e., at $z = 0$) as well as the electron viscosity effect expressed by $(1/e \langle n_e \rangle) \times \langle \nabla \cdot \mathbf{P}_e \rangle_y$ (blue curve). Figure 2(a) indicates that the dissipation mechanism at the x -line in 3D reconnection is very

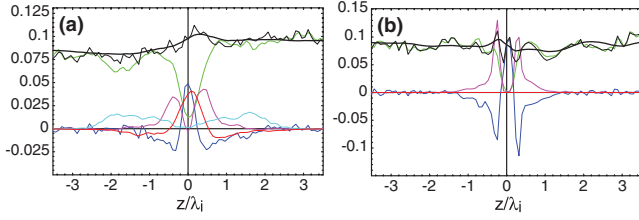


FIG. 2 (color). Contributions to the generalized Ohm's law [Eq. (1)] along the z axis through the x -line for (a) the 3D reconnection case at $t\omega_{ci} = 22.8$ and (b) the typical 2D reconnection case during the quasisteady period for comparison. Each curve shows $\langle -E_y \rangle$ (thick black curve), $(1/\langle n_e \rangle) \langle n_e \mathbf{V}_e \times \langle \mathbf{B} \rangle \rangle_y$ (green curve), $(1/e\langle n_e \rangle) \langle \nabla \cdot \mathbf{P}_e \rangle_y$ (blue curve), $(m_e/e\langle n_e \rangle) \times \langle n_e \mathbf{V}_e \cdot \nabla V_{ey} \rangle_y$ (purple curve), $(1/\langle n_e \rangle) \langle \delta n_e \delta E_y \rangle$ (light blue curve), $(1/\langle n_e \rangle) \langle \delta(n_e \mathbf{V}_e) \times \delta \mathbf{B} \rangle_y$ (red curve), and the summation of the right-hand side of Eq. (1) (thin black curve).

different from that in 2D reconnection [Fig. 2(b)] where the dissipation is provided only by the electron viscosity originating from the electron Speiser motion. It is also found that the electrostatic turbulence term $(1/\langle n_e \rangle) \langle \delta n_e \delta E_y \rangle$ (light blue curve) is negligibly small at the x -line. This suggests that the drag force due to the electrostatic potential hardly affects the dissipation at the x -line for the antiparallel configuration. The current sheet width is about two times larger in the 3D case than in the 2D case due to the EM turbulence. The turbulence thermalizes the electrons and increases the internal energy, so that the outflow velocity is decreased on average below the electron Alfvén velocity. The resultant electron layer has a larger aspect ratio (width per length) compared to that in the 2D case for the same reconnection rate.

The 2D profiles of the anomalous transport due to the EM turbulence are shown in Figs. 3(a)–3(c). One can see, in particular, in Fig. 3(c) that the EM turbulence is highly localized in a compact region around the x -line, which is the desirable condition for the Petschek-type fast reconnection [4]. It is important to notice that the EM turbulence at the x -line [red dots in Fig. 3(d)] evolves dynamically rather than remaining steady during the fast reconnection ($t\omega_{ci} \gtrsim 14$). Superposed on the EM turbulence effect in Fig. 3(d) is the distance L_{XO} along the x axis between the x -line and o -line of the plasmoids. We find that the enhancement of the EM turbulence is preceded by the plasmoid formations. Before the plasmoid formation [Fig. 3(a)], the turbulence is already dominant around the x -line, but the amplitude is relatively small. In association with the plasmoid formation, the turbulence is drastically enhanced locally around the plasmoid [Fig. 3(b)]. This is because the flow shear is enhanced in the flux rope for both species, which, as shown later, results in the increase in the growth rate of the EM mode responsible for the turbulence. In fact, Fig. 1(a) demonstrates that the wave amplitude is much larger in the plasmoid than in the thin current layer around the x -line. After the ejection of the plasmoid, it is

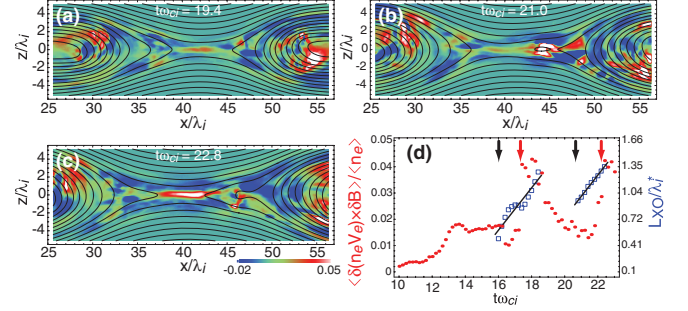


FIG. 3 (color). 2D profiles of the anomalous momentum transport due to the EM turbulence $(1/\langle n_e \rangle) \langle \delta(n_e \mathbf{V}_e) \times \delta \mathbf{B} \rangle_y$ at (a) $t\omega_{ci} = 19.4$, (b) $t\omega_{ci} = 21.0$, and (c) $t\omega_{ci} = 22.8$, and (d) time evolution of the anomalous transport at the instantaneous x -line (red dots) with the distance L_{XO} (blue squares) along the x axis between the x -line and o -line of the plasmoids, where L_{XO} is normalized by λ_i^* the local ion inertia length. The black lines in (d) represent the regression lines of L_{XO} for each plasmoid. The moments of the plasmoid generation and the enhancement of the turbulence at the x -line are indicated by black and red arrows, respectively, in (d).

observed that the turbulence is significantly enhanced around the x -line [Fig. 3(c)]. The time difference between the generation of the plasmoid and the enhancement of the turbulence at the x -line is estimated as $\Delta t \approx 1.6\omega_{ci}^{-1}$ for the second plasmoid. The plasmoid is located initially at $L_{XO} \approx 0.95\lambda_i^*$, where λ_i^* is the local ion inertia length. This indicates that the information has propagated from the o -line to the x -line with $V_p = L_{XO}/\Delta t \approx 0.59\lambda_i^*\omega_{ci} \approx 1.2V_A^*$, where V_A^* is the local Alfvén velocity based on B^* the magnetic field at the upstream edge of the electron current layer (here, $B^* \approx 0.5B_0$ around the flux rope). The same analysis leads to $V_p \approx 0.86V_A^*$ for the first plasmoid case. Therefore, it is reasonable to conclude that the turbulent electron flow pattern enhanced around the plasmoids propagates along the field lines and increases the turbulence at the x -line. In other words, the plasmoid formation in the x direction has a significant impact on the EM turbulence in the y direction.

We further investigate the linear properties of the EM mode responsible for the turbulent electron flow. The instabilities in the current layer have been studied intensively for the Harris-type current sheet [22–24] where the pressure and current density gradients are supported by the density gradients under the uniform temperature and bulk velocity. However, during the quasisteady reconnection, the profile is far from the Harris sheet. The density profile is almost uniform, so that the pressure and current density profiles are maintained through the temperature and bulk velocity gradients, respectively. Furthermore, the current sheet develops a two-scale structure consisting of the electron and ion current sheets. Therefore, it is very questionable that the previous results for the Harris sheet are still applicable in the quasisteady reconnection. The present study introduces a more realistic equilibrium with the

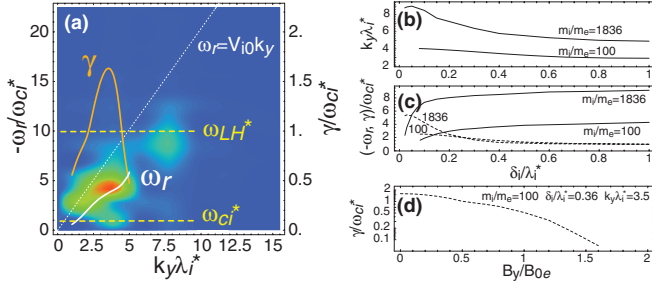


FIG. 4 (color). (a) Comparison in the ω - k diagram between the simulation results for B_x at the x -line during the fast reconnection in color contour and the linear analyses in solid curves (ω_r , the real frequency and γ the growth rate) with a wave dispersion propagating at V_{i0} in dotted curve. (b),(c) dependencies on δ_i for $m_i/m_e = 100$ and $m_i/m_e = 1836$ of (b) the wave number and (c) the frequencies (ω_r in solid curve and γ in dashed curve), and (d) dependency on the guide field of γ for $m_i/m_e = 100$. The local ω_{ci} and ω_{LH} are also indicated in (a).

two-scale structure based on the two-fluid equations. We assume the uniform number density n , the magnetic field $B_x(z) = -\sum_s B_{0s} \tanh(z/\delta_s)$, and the bulk velocity $V_s(z) = -V_{s0}/\cosh^2(z/\delta_s)$, where s indicates the species and there must be the relation $V_{s0} = (1/\mu_0 n q_s)(B_{0s}/\delta_s)$ for satisfying the Ampère's law. To maintain the pressure balance, the temperature has a spatial gradient so that $T_s(z) = -\int^z q_s V_s(\xi) B_x(\xi) d\xi$. The wave dispersion is obtained by solving the linearized two-fluid equations numerically using an initial value approach starting with small random noise [22].

Figure 4(a) shows the wave spectrum near the x -line in the simulation (color contour), which indicates that the EM mode has a frequency between ω_{ci}^* and ω_{LH}^* , consistent with the satellite observations in the geomagnetotail [13], where the asterisk denotes the local value using B^* . The linear properties presented by the solid curves are in good agreement with the simulation results, which demonstrates that the two-fluid approximation is valid for this EM mode, where the parameters used in the linear analyses are taken from the simulation results as $\delta_i = 0.36\lambda_i^*$, $V_{i0} = 2.1V_{Ae}^*$, $\delta_e = \lambda_e^*$, and $V_{e0} = V_{Ae}^*$ with λ_e^* and V_{Ae}^* the local values of the electron inertia length and the electron Alfvén velocity, respectively. The comparisons of the wave dispersion between the cases for $m_i/m_e = 100$ and $m_i/m_e = 1836$ are given in Figs. 4(b) and 4(c). Since there is theoretical ambiguity in determining δ_i the width of the ion current sheet, we check the dependencies on δ_i . We find that the growth rate (dashed curve) converges on $\gamma \sim \omega_{ci}^*$ in both the cases, almost independent of the mass ratio. This indicates that the EM mode survives even in the real mass ratio limit. It is interesting to note that, although the peak velocities V_{i0} and V_{e0} are fixed through the analyses, the growth rate decreases as δ_i increases. This suggests that the mode is driven by the velocity shear of the ions rather than the relative drift velocity between the

species as has been argued in the previous studies [22,23]. The mode also differs from the ion-ion kink mode [24] because k_y and ω_r have a mass ratio dependence, so that both the species are coupled. The EM mode is stabilized drastically with guide field [Fig. 4(d)], which implies that the mode hardly affects the reconnection process under intense guide field ($B_y/B_{0e} \gtrsim 1$). Thus, the dissipation mechanism in antiparallel reconnection is different from that in guide-field reconnection [18].

Our 3D simulation and linear analyses demonstrate that the EM turbulence plays a significant role in the magnetic dissipation during quasisteady period in antiparallel reconnection with the help of the plasmoid formations. The direct impact of the anomalous momentum transport appears in the current sheet width [14]. The average width for the 3D case is about two times larger than that for the 2D case. However, the observations in space and laboratory plasmas have shown even wider current layers during the fast reconnection [10,11], which suggests the existence of more intense turbulence. A more turbulent current layer may be achieved in the nonlinear phase of the EM mode after the longer time evolution. The present study will be helpful for NASA's upcoming Magnetospheric Multi-Scale mission to specify the dissipation mechanism in the geomagnetotail reconnection.

The simulations were carried out by Fujitsu FX1 installed at the ITC, Nagoya University, with support from the HPC joint research project at Nagoya University and a computational joint research program at the STE Laboratory, Nagoya University. The present work has been also supported by the JSPS Grant-in-Aid for Young Scientists (B) (23740373). K.F. appreciates the Special Postdoctoral Researchers Program at RIKEN.

*keizo.fujimoto@nao.ac.jp

- [1] E. N. Parker, *J. Geophys. Res.* **62**, 509 (1957).
- [2] P. A. Sweet, in *Electromagnetic Phenomena in Cosmical Physics*, edited by B. Lehnert (Cambridge University Press, London, 1958), p. 123.
- [3] D. Biskamp, *Phys. Fluids* **29**, 1520 (1986).
- [4] M. Ugai, *Phys. Plasmas* **2**, 388 (1995).
- [5] J. Raeder, R. L. McPherron, L. A. Frank, S. Kokubun, G. Lu, T. Mukai, W. R. Paterson, J. B. Sigwarth, H. J. Singer, and J. A. Slavin, *J. Geophys. Res.* **106**, 381 (2001).
- [6] M. M. Kuznetsova, M. Hesse, L. Rastätter, A. Taktakishvili, G. Toth, D. L. D. Zeeuw, A. Ridley, and T. I. Gombosi, *J. Geophys. Res.* **112**, A10210 (2007).
- [7] T. W. Speiser, *Planet. Space Sci.* **18**, 613 (1970).
- [8] H. J. Cai and L. C. Lee, *Phys. Plasmas* **4**, 509 (1997).
- [9] M. Hesse, K. Schindler, J. Birn, and M. Kuznetsova, *Phys. Plasmas* **6**, 1781 (1999).
- [10] H. Ji, Y. Ren, M. Yamada, S. Dorfman, W. Daughton, and S. P. Gerhardt, *Geophys. Res. Lett.* **35**, L13106 (2008).
- [11] J. R. Wygant *et al.*, *J. Geophys. Res.* **110**, A09206 (2005).

- [12] J. P. Eastwood, T. D. Phan, S. D. Bale, and A. Tjulin, *Phys. Rev. Lett.* **102**, 035001 (2009).
- [13] M. Zhou *et al.*, *J. Geophys. Res.* **114**, A02216 (2009).
- [14] V. M. Vasyliunas, *Rev. Geophys.* **13**, 303 (1975).
- [15] Z. Zhu and R. M. Winglee, *J. Geophys. Res.* **101**, 4885 (1996).
- [16] R. Horiuchi and T. Sato, *Phys. Plasmas* **6**, 4565 (1999).
- [17] A. Zeiler, D. Biskamp, J. F. Drake, B. N. Rogers, M. A. Shay, and M. Scholer, *J. Geophys. Res.* **107**, 1230 (2002).
- [18] H. Che, J. F. Drake, and M. Swisdak, *Nature (London)* **474**, 184 (2011).
- [19] K. Fujimoto, *Phys. Plasmas* **13**, 072904 (2006).
- [20] W. Daughton, J. Scudder, and H. Karimabadi, *Phys. Plasmas* **13**, 072101 (2006).
- [21] K. Fujimoto, *J. Comput. Phys.* **230**, 8508 (2011).
- [22] P. L. Pritchett, F. V. Coroniti, and V. K. Decyk, *J. Geophys. Res.* **101**, 27 413 (1996).
- [23] H. Suzuki, M. Fujimoto, and I. Shinohara, *Adv. Space Res.* **30**, 2663 (2002).
- [24] H. Karimabadi, W. Daughton, P. L. Pritchett, and D. Krauss-Varban, *J. Geophys. Res.* **108**, 1400 (2003).